

# Aperiodicity Correction for Rotor Tip Vortex Measurements

Manikandan Ramasamy\*

University Affiliated Research Center

NASA Ames Research Center

Moffett Field, CA 94035

Ryan Paetzel†

Aeromechanics Branch

NASA Ames Research Center

Moffett Field, CA 94035

Mahendra J. Bhagwat‡

Aeroflightdynamics Directorate

U. S. Army Research, Development, and Engineering Command (AMRDEC)

Moffett Field, CA 94035

The initial roll-up of a tip vortex trailing from a model-scale, hovering rotor was measured using particle image velocimetry. The unique feature of the measurements was that a microscope was attached to the camera to allow much higher spatial resolution than hitherto possible. This also posed some unique challenges. In particular, the existing methodologies to correct for aperiodicity in the tip vortex locations could not be easily extended to the present measurements. The difficulty stemmed from the inability to accurately determine the vortex center, which is a prerequisite for the correction procedure. A new method is proposed for determining the vortex center, as well as the vortex core properties, using a least-squares fit approach. This approach has the obvious advantage that the properties are derived from not just a few points near the vortex core, but from a much larger area of flow measurements. Results clearly demonstrate the advantage in the form of reduced variation in the estimated core properties, and also the self-consistent results obtained using three different aperiodicity correction methods.

## Nomenclature

$a_n, b_n$	Constants
$c$	Blade chord, mm
$C_T$	Rotor thrust coefficient
$L_m$	Measurement window size, mm
$r$	Radial distance from the vortex center, mm
$r_c$	Vortex core radius, mm
$R$	Rotor radius, mm
$[R_x], [R_y]$	Transformation matrices for rotational angles
$u, v$	Velocity components along $x$ - and $y$ -axis, $\text{ms}^{-1}$
$u_c, v_c$	Vortex convection velocities, $\text{ms}^{-1}$
$V_\theta$	Swirl velocity, $\text{ms}^{-1}$
$x, y, z$	Measurement coordinate system, mm
$x_c, y_c$	Vortex center location, mm
$\Gamma_v$	Vortex circulation, $\text{mm ms}^{-1}$
$\theta_x, \theta_y$	Vortex axis orientation angles, deg
$\mu$	Mean
$\sigma$	Standard deviation
$\psi$	Wake age, deg

\* Research Scientist. [mani.ramasamy@us.army.mil](mailto:mani.ramasamy@us.army.mil)

† EAP Intern, [rmp88@vt.edu](mailto:rmp88@vt.edu)

‡ Research Scientist. [mahendra.bhagwat@us.army.mil](mailto:mahendra.bhagwat@us.army.mil)

Presented at the AHS 67<sup>th</sup> Annual Forum, Virginia Beach, VA, May 3–5, 2011. This material is declared a work of the U. S. Government and is not subject to copyright protection in the United States.

## Introduction

A helicopter rotor wake is a complex, three-dimensional, and inherently turbulent flow field. Advanced optical measurement techniques such as Laser Doppler Velocimetry (LDV) and Particle Image Velocimetry (PIV) have been employed to accurately measure the wake flow field. However, one key aspect of the rotor wake poses a unique challenge for all ground-fixed measurement techniques. Tip vortices trailing from both fixed- and rotary-wing tips exhibit small random motion normal to the vortex axis. This wandering motion is often referred to as “aperiodicity” by the rotorcraft community, because the motion represents the variation or scatter in the vortex center location from one period (rotor revolution) to another. Whatever the source of this aperiodicity, it is important to understand the movement of the vortex center location because of its profound effect on the local blade loading. Apart from this loading effect, the aperiodicity also has a strong effect on the mean tip vortex properties estimated from the flow field measurements. The aperiodicity introduces an artificial smearing effect when averaging to obtain mean flow properties, resulting in a larger apparent core size and a smaller peak swirl velocity. This smearing effect due to aperiodicity also occurs with point measurement techniques such LDV and Hot-

Wire Anemometry (HWA), see, e.g., Refs. 1–5. Furthermore, for such point measurement techniques separating the velocity variations caused by turbulence and aperiodicity is difficult (Ref. 5).

To illustrate the effects of vortex aperiodicity, four instances of tip vortex measurements are shown in Fig. 1. The vortex core is seen as a data void because of the difficulty in seeding the flow in the core. With a fixed measurement window, large variations in the vortex center location are readily apparent. The circles represent the approximate vortex core boundaries corresponding to the local maxima in swirl velocity. When a number of such individual images are averaged to obtain mean flow properties, the resulting flow field will be smeared because of the aperiodicity or wandering of the vortex centers. This is clearly seen in Fig. 2(a). The averaged flow field shows a vortex that is larger in size with lower swirl velocity than any of the instantaneous measurements.

A better approach for obtaining the mean flow characteristics is to first align the instantaneous measurements using their vortex centers. In this case, the averaging does not produce the smearing effect. This is evident from Fig. 2(b), where the averaged vortex looks nearly the same size as the instantaneous measurements. This is the central idea of the aperiodicity correction method applied to PIV measurements.

For point measurement techniques like LDV or HWA, such center alignment is not possible because measurements are averaged at each point separately. In this case a different correction techniques would be necessary. Devenport et al. (Ref. 5) analyzed the effects of aperiodicity on the measured vortex core properties using convolution of the Lamb-Oseen vortex model (Ref. 6, 7) with an assumed Gaussian wandering motion. This results in an apparent or measured core size that is larger than the actual vortex core, similar to the larger core seen in Fig. 2(a). The results of this analysis are shown in Fig. 3 in the form of ratios of measured to actual vortex core radius and peak swirl velocity. This essentially gives a correction factor that can be applied to the averaged flow field, such as the one shown in Fig. 2(a). Leishman (Ref. 8) developed a similar numerical deconvolution procedure that uses measured velocity profiles instead of an assumed Lamb-Oseen vortex profile.

Simple averaging with such an analytical or numerical correction has been successfully applied to rotor tip vortex measurements using LDV (Refs. 2, 3). Later PIV measurements, however, did not employ this approach, and only reached the obvious conclusion that the simple average (without any subsequent correction) does not give a good estimate of vortex properties. It should be noted that such correction is practical only when the scatter in spatial location is less than one core diameter, because for larger scatter the averaged flow field does not even resemble the underlying vortex induced

flow. Instead, tip vortex PIV measurements used the corrected average or conditional average, where instantaneous measurements were averaged after aligning their respective vortex centers (Refs. 9–15).

Several criteria for determining the vortex center have been used in the past and these include: node location of maximum vorticity (Refs. 9–12), centroid of flow invariants like vorticity,  $\lambda_2$ ,  $Q$ -criterion (Refs. 14, 15), or helicity (Ref. 14). Reference 15 showed improved accuracy in obtaining the vortex center using the convolution of measurements with a discrete mask based on an assumed vortex model. This approach was shown to reduce scatter in the estimated vortex core properties.

Another approach only possible with PIV measurements is to analyze the instantaneous vector fields itself to estimate the instantaneous vortex core properties. Subsequently, hundreds of individual vortex core properties are then averaged to obtain mean values (Refs. 9, 12, 15). The obvious advantage of this method is that it does not require computing an averaged flow field. While Ref. 15 showed that it gave essentially the same values of vortex core properties as the conditional average, results from Refs. 9 and 12 yielded different values between these two methods.

To better understand these inconsistencies, it is essential to examine the different methods used for obtaining the vortex core properties from the corrected average (or even from the instantaneous) flow field. Initial PIV measurements appeared to have followed their LDV/HWA predecessors in using only horizontal and vertical cuts through the vortex center to determine the vortex core properties. This was done simply based on the locations of peak swirl velocity in Refs. 9 and 13. Ref. 15 used a planar curve-fit to obtain the vortex core properties.

The objective of the present study is to compare and contrast the different approaches to aperiodicity correction together with the methods for estimating core properties using a single set of measurements. This paper describes the PIV measurements, the methodology for the aperiodicity correction, results of applying the methodology to the measurements, and major conclusions.

## Description of Experiment

The measurements used in the present study were performed on a three-bladed model-scale rotor system with a highly-twisted rotor blade that was similar to the XV-15 blade. The blade had a radius of 656 mm and 49 mm chord. Measurements at two thrust levels ( $C_T = 0$  and  $C_T = 0.0076$ ) are used in the present study. For the highly twisted rotor blade, the zero thrust case is of interest because of the presence of a strong opposite-spinning tip vortex. A schematic of the experimental setup is shown in Fig. 4 and further details can be found in Ref. 16.

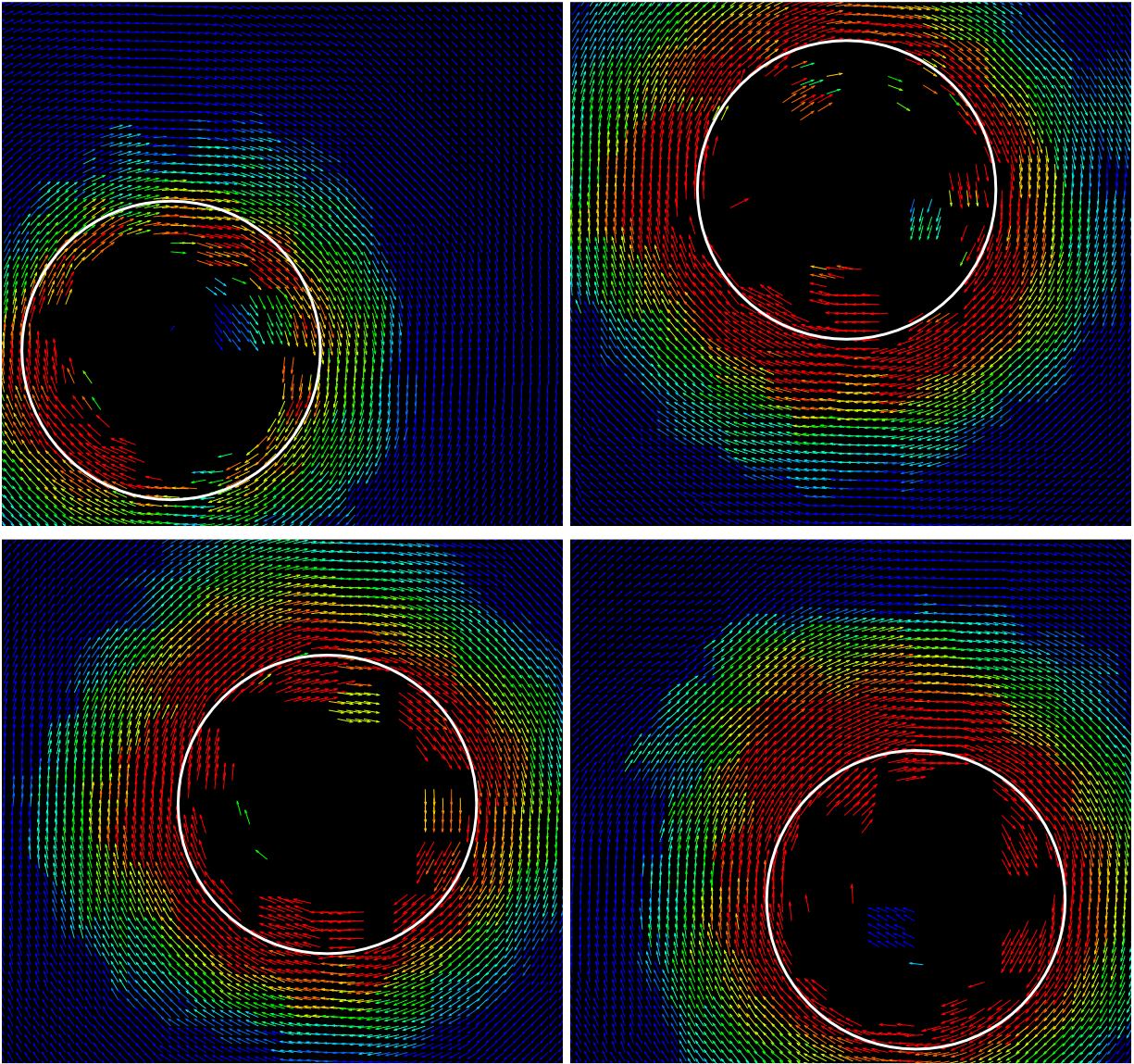


Fig. 1. Four instances of measured flow field exhibiting aperiodicity in rotor tip vortices. Velocity vectors are colored using the velocity magnitude.

(a) Simple average of measured flow fields

(b) Flow fields averaged with centers aligned

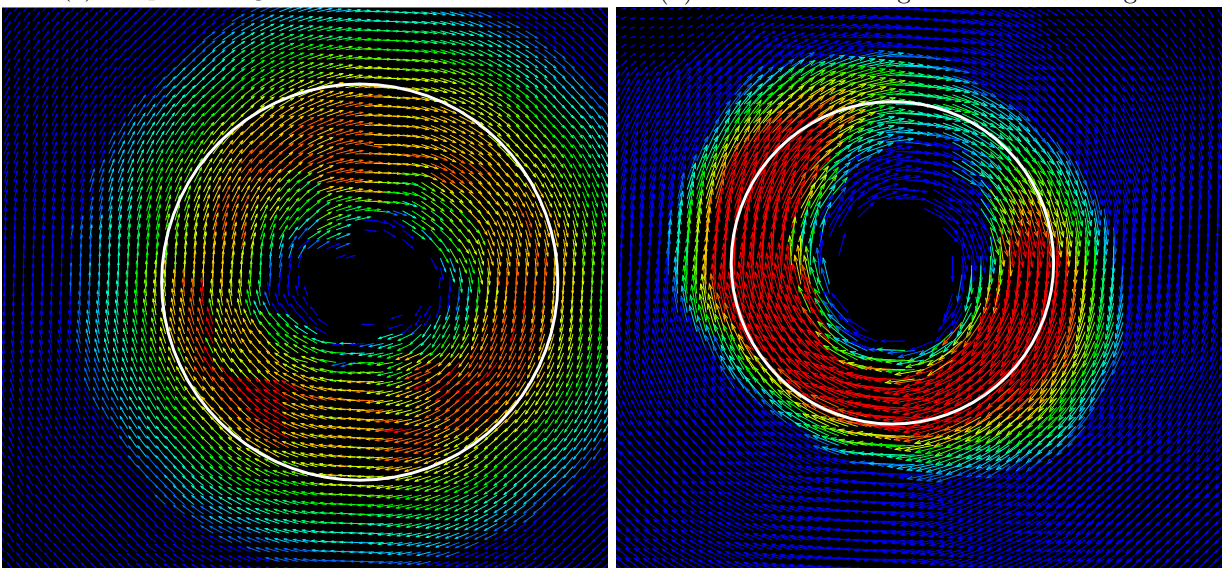
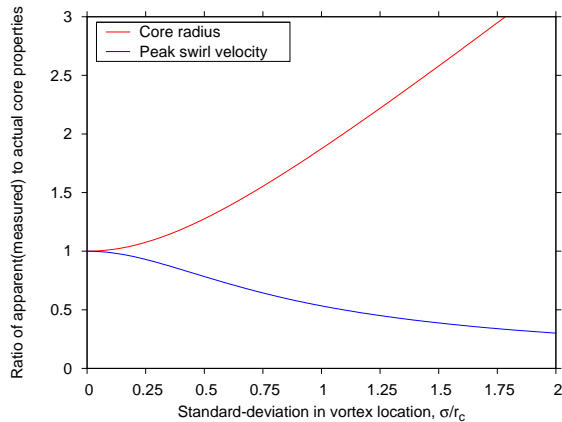
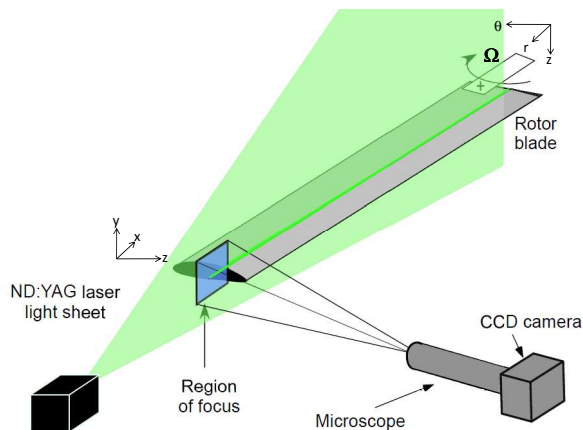


Fig. 2. Effects of tip vortex aperiodicity in the averaged flow field



**Fig. 3. Analytical correction for vortex aperiodicity by Deavenport et al. (Ref. 5)**



**Fig. 4. Schematic of the experimental setup**

The unique feature of these PIV measurements was that the camera was fitted with a microscope that enabled a field of view as small as  $24 \times 18$  mm. As a result, very high resolution measurements were possible with 18–27 independent measurement points along one vortex core diameter. With 50% overlap, as used in the present study, this corresponded to 36 vectors across the vortex diameter at the earliest measured wake age ( $4^\circ$ ) and 54 vectors at the oldest wake age ( $15^\circ$ ). A high signal-to-noise ( $\text{SNR} \geq 2$ ) was specified resulting in only a few, but statistically valid, measurements inside the vortex core.

A comparison of the resolution with some previous tip vortex measurements is shown in Table 1. Similar to the Table 1 in Ref. 15, the ratio of measurement window to the core radius,  $L_m/r_c$  is calculated assuming a 0.05  $c$  core radius rather than the actual value.

## Methodology

Tip vortex aperiodicity correction methods can be classified into three categories: the simple average (SA), the corrected average or conditional average (CA), and the

**Table 1. Tip vortex measurements resolution**

Experiment	$L_m/r_c$	Independent points within core diameter
UMD (Ref. 14)	0.22	8–18
TRAM (Ref. 9)	1.83	3–6
HART-II (Ref. 15)	0.51	3–5
Present work	0.08	18–27

individual average (IA). Figure 5 shows these three methods, and identifies key steps involved in each. The common step in each method is the determination of vortex core properties from either the averaged or the instantaneous flow field. For the CA method, the vortex center for each individual measurement must be determined prior to determining the vortex core properties from the averaged flow field. In fact, it is suggested that the accurate estimation of the vortex center is necessary for the accurate estimation of the vortex core properties (Ref. 15).

## Vortex Center

The most common methods to calculate the vortex center from measured flow field, as mentioned earlier, are based on the centroid of flow invariant property like vorticity,  $\lambda_2$ ,  $Q$ -criterion, etc. Ideally the vortex center defined by any of these criteria would be the same. However, in reality the vortex center estimates do not always agree (Ref. 12, 15, 17). One short-coming of all of these approaches is that they rely mostly on measurements near the vortex core where reliable measurements are difficult to make. This is because of the difficulties in getting enough seed in the vortex core (Ref. 18) together with higher variations in velocity due to turbulence. As a result the measurements near the vortex core have a lower confidence level, and contribute to errors in the estimated vortex center location. Eliminating the measurements with low confidence levels simply results in a data void near the vortex center. In the present measurements, the strict signal-to-noise ratio limits imposed on the PIV data resulted in a data void region, which was often as big as the vortex core itself (see Fig. 1).

PIV processing software often fills such data voids using interpolated values from surrounding measurements. As the velocity inside the vortex core is almost linear, this interpolation may not be a problem. However, if the void is not symmetric then the interpolated values may introduce errors in calculating the vortex center. This is shown in Fig. 6 using tip vortex measurements at two different instances. The white circle represents the core that is visually identified based on maximum swirl velocity, with its center being shown by the cross. The vortex centers identified using centroid of vorticity,  $Q$ -criterion and  $\lambda_2$  are shown using circle, square and triangle, respectively. For an axisymmetric vector void, as seen in Fig. 6(a), the centers estimated from all three quanti-

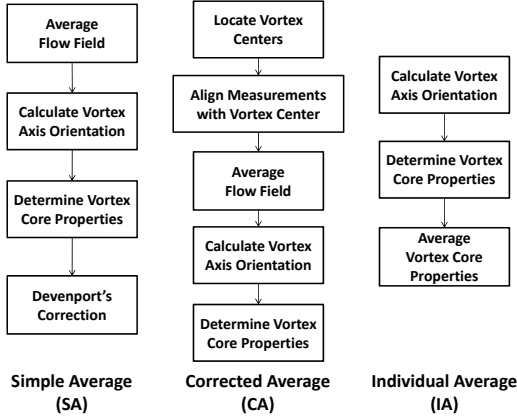


Fig. 5. Tip vortex aperiodicity correction methods

ties agree with each other. However, when the void is asymmetric the centers determined by different methods vary significantly, and are offset from the actual center away from the void as seen in Fig. 6(b). Clearly, devising a method that is not affected by such a void near the vortex core is necessary.

The convolution approach used in Ref. 15 showed improved accuracy in estimating the vortex center. Although the measurements reported in Ref. 15 did not show a data void near the center, the approach definitely demonstrated the benefit of using a larger measured flow field rather than only a few measurement points inside the vortex core. Subsequently, a curve fit to the measurement plane was made to determine the vortex core properties based on the Vativistas vortex model (Ref. 19). The present method combines these two approaches into a least-squares fit to the entire measurement plane (all velocity data) to obtain not just the vortex core properties, but also the vortex center and the vortex convection velocity. Note that maximizing the convolution of measurements with an assumed distribution is, in principle, similar to a least-squares fit where the difference between the measurements and an assumed distribution is minimized.

### Least-Squares Fit with a Vortex Model

The present approach is based on a least-squares fit of the measured velocities to those given by an assumed vortex model. In general, the measurement plane is not normal to the vortex axis. Therefore, the vortex axis orientation relative to the measurement plane must be taken into account to correctly identify the vortex core properties. A transformation is required between the measurement coordinate system  $(x, y, z)$  and the vortex coordinate system,  $(x_v, y_v, z_v)$ . The vortex axis is aligned with the  $z_v$ -axis and positive circulation,  $\Gamma_v$ , is defined by the right-hand-rule. In the present analysis only a swirl velocity model is used and is defined as a function of the radial

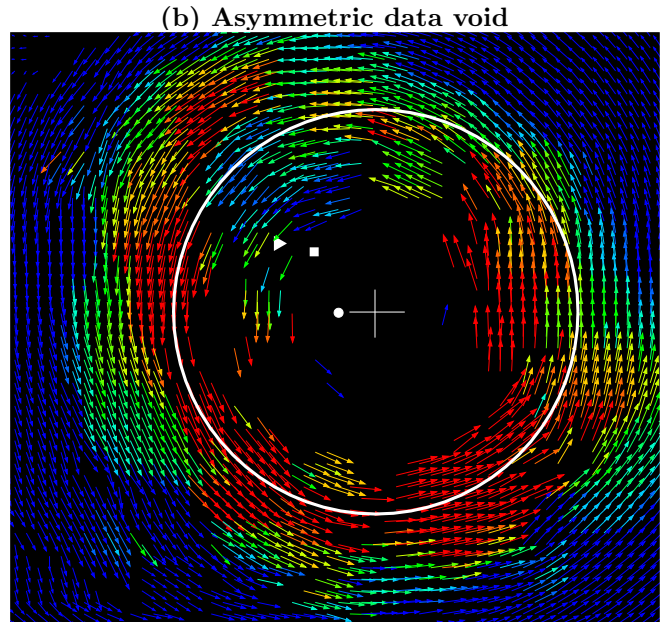
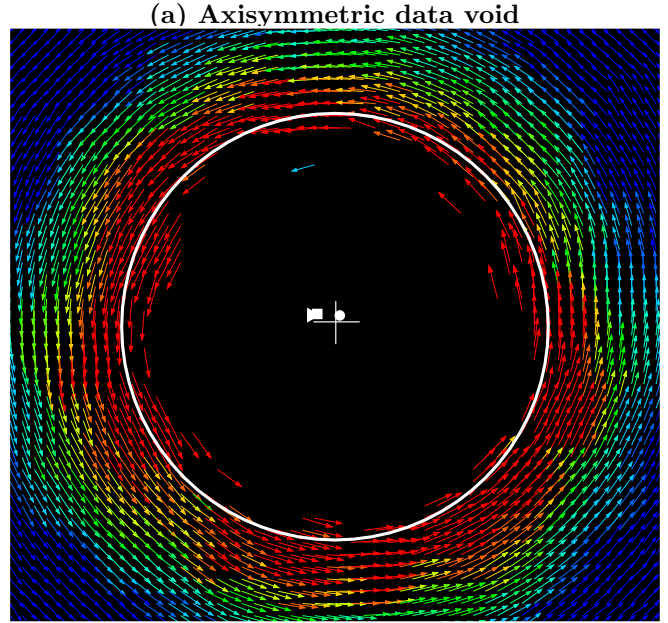
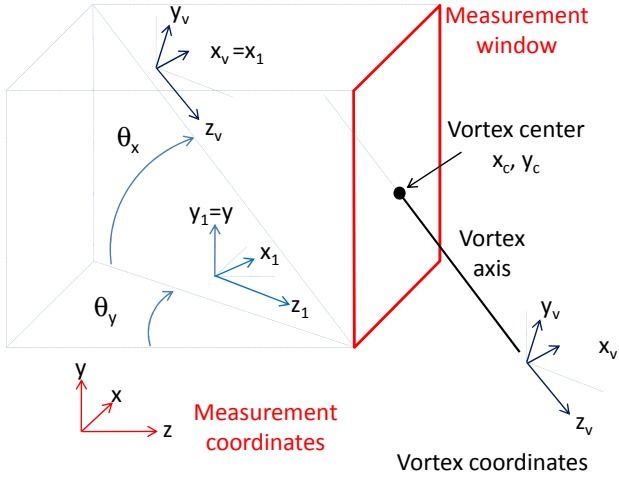


Fig. 6. Variation in the vortex center based on various vortex properties with (a) Axisymmetric data void, and (b) Asymmetric data void;  $\bullet$  corresponds to the centroid of vorticity,  $\blacksquare$  to  $Q$ -criterion, and  $\blacktriangleright$  to  $\lambda_2$ .

distance,  $r_v$ , from the vortex center, along with a core radius,  $r_c$ , and the vortex circulation,  $\Gamma_v$ .

The center of the vortex  $(x_c, y_c)$  is defined in the measurement coordinates,  $(x, y, z)$ . The vortex convection velocity or background velocity is represented by  $(u_c, v_c)$ , also in the measurement coordinates. Two rotation angles are required to transform from the measurement coordinates to the vortex coordinates. This is schematically shown in Fig. 7 where the PIV measurement window shown earlier in Fig. 4 is shown along with the measurement and vortex coordinates. A first rotation of  $\theta_y$  around the  $y$ -axis results in an intermediate coordinates



**Fig. 7. Inclination of vortex axis included through vortex convection velocities**

$(x_1, y_1, z_1)$  and a subsequent rotation  $\theta_x$  around the  $x_1$ -axis gives the vortex coordinates. The transformation matrices are given by

$$R_y = \begin{bmatrix} \cos \theta_y & 0 & -\sin \theta_y \\ 0 & 1 & 0 \\ \sin \theta_y & 0 & \cos \theta_y \end{bmatrix} \quad (1)$$

$$R_x = \begin{bmatrix} 1 & 0 & 0 \\ 0 & \cos \theta_x & \sin \theta_x \\ 0 & -\sin \theta_x & \cos \theta_x \end{bmatrix} \quad (2)$$

The transformation from the measurement coordinates to the vortex coordinates is then given by

$$\begin{Bmatrix} x_v \\ y_v \\ z_v \end{Bmatrix} = [R_x][R_y] \begin{Bmatrix} x - x_c \\ y - y_c \\ z \end{Bmatrix} \quad (3)$$

The vortex swirl velocity is transformed to the Cartesian vortex coordinates as

$$\begin{aligned} u_v &= -V_\theta \sin \theta = -V_\theta \frac{x_v}{r_v} \\ v_v &= V_\theta \cos \theta = V_\theta \frac{y_v}{r_v} \end{aligned} \quad (4)$$

These velocities are then transformed back to the measurement coordinates using the inverse transform. The resulting vortex function is given by

$$\mathbf{f}(r_c, \Gamma_v, x_c, y_c, u_c, v_c, \theta_x, \theta_y) =$$

$$V_\theta(r_v, r_c, \Gamma_v) [R_y]^T [R_x]^T \begin{Bmatrix} -\frac{x_v}{r} \\ \frac{y_v}{r} \\ 0 \end{Bmatrix} + \begin{Bmatrix} u_c \\ v_c \\ 0 \end{Bmatrix} \quad (5)$$

where the distance from the vortex center is

$$r_v = \sqrt{x_v^2 + y_v^2} \quad (6)$$

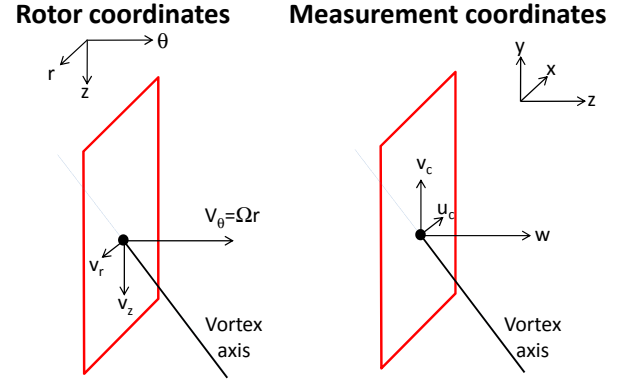


**Fig. 8. Inclination of vortex axis included through vortex convection velocities**

The least-squares fit uses the above function with the eight independent variables, viz.  $r_c, \Gamma_v, x_c, y_c, u_c, v_c, \theta_x, \theta_y$ , to obtain the best match with measured velocities, least error between the measurements and the fit.

A simpler special case of this least-squares fit is possible for the present measurements because the measurement plane coincides with a constant-azimuth,  $r-z$  plane in the blade-fixed coordinate system – see Fig. 8. As the vortices convect with the local flow velocity (the central premise of all free vortex wake methods), the vortex trajectory and the orientation of the vortex axis is determined by the local flow vector. In blade-fixed coordinates, at any point in space there is an apparent flow velocity of  $v_\theta = \Omega r$ . As the measurement plane coincides with the  $r-z$  plane, this velocity contributes to the  $z$ -component of velocity in the measurement plane. Therefore, the orientation angles can be readily expressed in terms of the vortex convection velocity components ( $u_c, v_c, \Omega r$ ) as

$$\theta_y = \arctan\left(-\frac{u_c}{\Omega r}\right) \quad \theta_x = \arctan\left(\frac{v_c}{\sqrt{\Omega^2 r^2 + u_c^2}}\right) \quad (7)$$

This simplification results in a least-squares fit with only six independent parameters, viz.  $r_c, \Gamma_v, x_c, y_c, u_c, v_c$ .

### Effect of measurement window size

To ensure that the least-squares fit method provides results independent of the choice of the window size, data was analyzed using a series of increasing subsets of measurements centered around the vortex. The subset size was varied from  $80 \times 80$  to  $240 \times 240$  nodes (i.e., approximately  $8 \times 8$  mm to  $24 \times 24$  mm) as shown in Fig. 9. The rotor induced velocity field varies significantly along both the radial and axial directions. The least-squares fit assumes a constant background velocity (or vortex convection velocity), and the measurement subset must be small to justify this assumption. On the other hand, the subset must be large enough compared to the vortex core

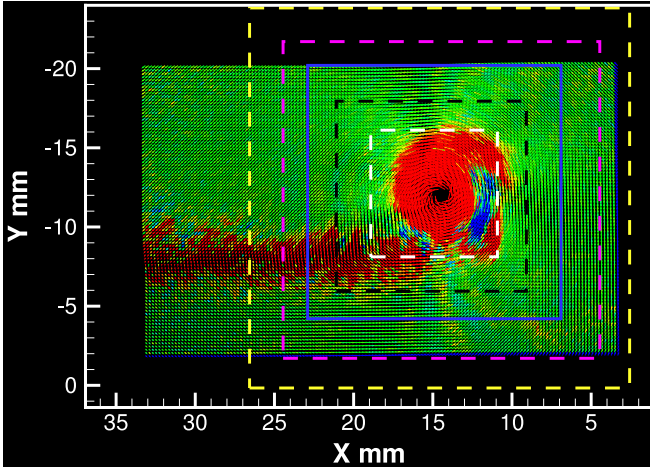


**Fig. 9.** Data subsets of various size centered around the vortex used in the least-squares fit.  $C_T = 0.0076$ ,  $\psi = 4$  deg.

to ensure that all the vortex circulation is considered. These contradicting requirements are met relatively easily when using least-squares function fit approach.

At early wake ages the inner wake sheet is present in close proximity to the tip vortex, and a small enough window should be chosen to eliminate its influence on the result. This is evident in Fig. 9 where a measured PIV flow field is shown as velocity vectors colored by the vorticity. The inner wake sheet is clearly evident. More and more of the inner wake sheet is included in the least-squares fit with increasing subset. To eliminate the effects of such extraneous flow features on the estimated vortex core properties, the individual measurements that showed a difference of greater than 2% in vortex circulation between the largest three window sizes were not included in the analysis. Only about 2–3% of the measurements did not meet this window-size independence criterion.

### Vortex Profile Model

To perform a least-squares fit to the function  $\mathbf{f}$  as defined above, a suitable vortex velocity profile model for swirl velocity distribution must be chosen. The choice of this model is important because the resulting vortex core properties may well be biased by the choice. Several vortex profile models are available in the literature, and the initial choices used in the present study are based on solutions to the Navier-Stokes equations with varying levels of simplifying assumptions. These models include a potential vortex (or Rankine vortex) where all the circulation is contained inside the vortex core, a laminar Lamb-Oseen vortex (Ref. 6, 7) where about 70% circulation is contained in the core, a fully turbulent model by Iversen (Ref. 20) where only about 40% circulation is contained in the core, as well as a transitional model proposed by Ramasamy and Leishman (Ref. 21) which is

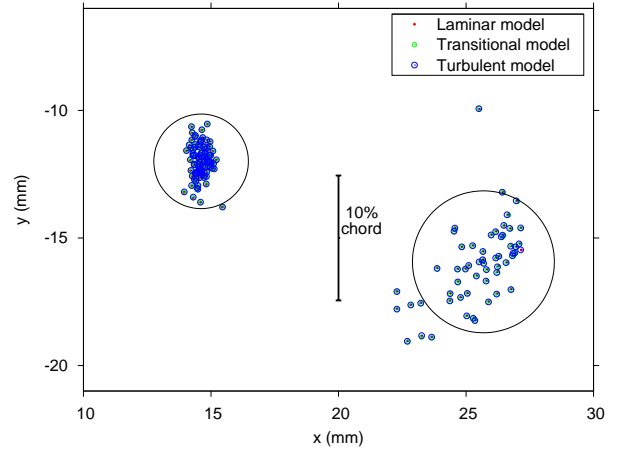


**Fig. 10.** The vortex center locations estimated using three vortex models.  $C_T = 0.0076$ ,  $\psi = 4$  deg and 15 deg. in between the laminar and the fully turbulent models. The Lamb-Oseen model is given by

$$V_\theta = \frac{\Gamma_v}{2\pi r} \left( 1 - \exp\left(-\alpha (r/r_c)^2\right) \right) \quad (8)$$

where  $\alpha = 1.25643$ . The Iversen and the transitional models are not closed-form solutions but are formulated as solutions to an ordinary differential equation. Reference 22 presents an approach to approximately represent these models as a weighted average of three Lamb-Oseen type vortex profiles with different core radii, i.e.,

$$V_\theta(r, r_c, \Gamma_v) = \frac{\Gamma_v}{2\pi r} \left[ 1 - \sum_{n=1}^3 a_n \exp(-b_n (r/r_c)^2) \right] \quad (9)$$

$$\text{with } \sum_{n=1}^3 a_n = 1.$$

Figure 10 shows the vortex centers identified using the three vortex models (laminar, transitional and turbulent) for two vortex ages ( $\psi = 4^\circ, 14^\circ$ ). The younger vortex on the left shows smaller aperiodicity (variation in the location) while the slightly older vortex on the right shows larger aperiodicity. However, in both cases the centers identified using all three models are almost identical. Although surprising, this is not totally unexpected because these vortex models differ only in a region close to the center. Away from the center all models exhibit essentially the same behavior, and can correctly identify the center of rotation of the flow. This can be seen even more clearly by looking at velocity and circulation distribution given by these models.

Figure 11a and b show the measured swirl velocity and circulation distribution along horizontal and vertical cuts through the vortex centers after subtracting  $u_c$  and  $v_c$  (laminar model used here). Profiles from the laminar, transitional and turbulent vortex models, as well as the potential vortex and the Rankine vortex model are also shown. As mentioned earlier, the ratio of the core circulation to the total vortex circulation is different for each

of these models. As a result, the core radius and the peak swirl velocity estimated from these models are also different. The Rankine vortex gives the largest core radius with the laminar, transitional and turbulent models showing progressively smaller core radius.

More importantly, it appears as though all the models are under-predicting the measured peak swirl velocity. Remember, the measurements shown here are just from horizontal and vertical cuts, but the curve fit is made to the entire PIV plane. This means that there must be several other cuts through the center of the vortex (other than horizontal and vertical) that must be providing lower values of peak swirl velocity. Figure 11 is shown only to compare the capability of the models to identify the center of the vortex and not to evaluate their abilities to estimate the core properties.

The vortex core properties are clearly influenced by the choice of the vortex model. However, from Fig. 10, it is important to note that the center identification is independent of the choice of the vortex model used in the curve fitting algorithm.

The Iversen model (Ref. 20) as well as the transitional model (Ref. 21) change with vortex Reynolds number and it would be possible to adapt either of these models based on the vortex Reynolds number estimated using the least-squares fit. The present measurements were performed on a small-scale rotor at very early wake ages. Therefore, the vortex was more or less laminar, and the measured velocity profiles closely resembled the Lamb-Oseen vortex. Even the Iversen and transitional models for the low vortex Reynolds number for the present experiments were almost the same as the laminar model. Therefore, Lamb-Oseen model was used for all further analyses in this paper.

### Conditional Average

The individual measurements are aligned using the vortex center locations as determined above and then averaged to obtain a mean flow field. In general, the vortex center does not lie on a measurement grid node and alignment requires re-meshing and interpolation of the measured data. When the grid spacing is a relatively large fraction of the vortex core radius, interpolation must be used (see, e.g., Ref. 15). If the grid spacing is a small fraction of the core radius then the individual measurements can be aligned simply using the grid node closest to the vortex center. This results in a residual aperiodicity in the measurements, which is less than half the diagonal grid spacing. In the present study, the measurement grid spacing was less than 5% of the core radius. Therefore, using the grid node closest to vortex center resulted in a very small residual aperiodicity (see Fig. 12) in the averaged measurements. Based on analysis by Devenport et al. (Ref. 5) this would result in less than 0.1% error

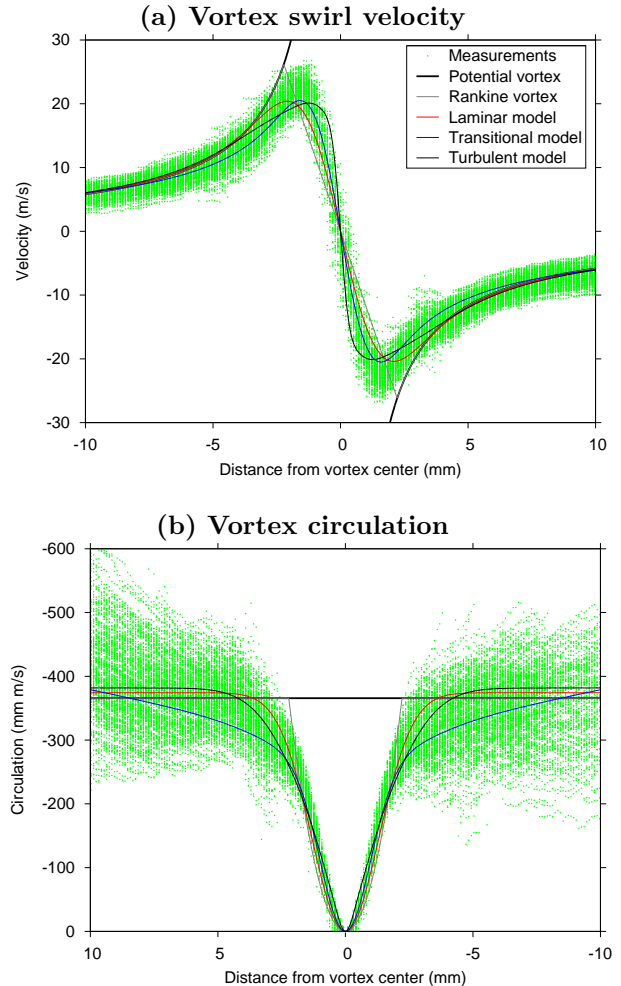


**Fig. 11. Measured swirl velocity and circulation distributions along horizontal and vertical cuts through the vortex center. Different vortex models are also shown for comparison.  $C_T = 0.0$ ,  $\psi = 4$  deg.**

in the measured peak swirl velocity and the core radius. Therefore, alignment based on the grid node closest the vortex center was followed in the present work.

Swirl velocity and circulation profiles along horizontal and vertical cuts through the vortex center from the corrected average are shown in Fig. 13(a) and (b), respectively, along with similar cuts from all individual measurements. In this case only the vortex center obtained from the least-squares fit is used. The vortex core properties are obtained from the horizontal/vertical cuts based on the measured peak swirl velocities, identified in the figure using solid black circles. The core radius is given by half the distance between the two peaks, the peak swirl velocity is given by the half peak-to-peak velocity, while the vortex convection velocity is given by the average of the two peaks. This estimation of core properties using line cuts may be rooted in earlier measurement techniques like LDV/HWA. However, using only two cuts through the vortex center is a gross under-utilization of planar PIV data. Having obtained measurements over an entire grid, only four points from the averaged mea-

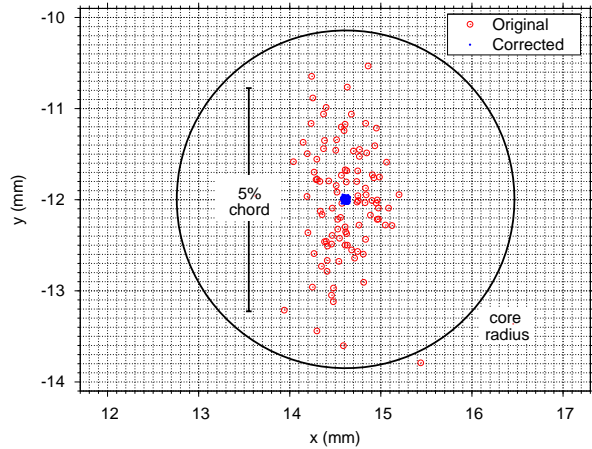


**Fig. 12. Small residual aperiodicity when measurements are aligned using the node closest to the vortex center,  $C_T = 0.0076$ ,  $\psi = 4$  deg. Grid lines correspond to the the measurement grid.**

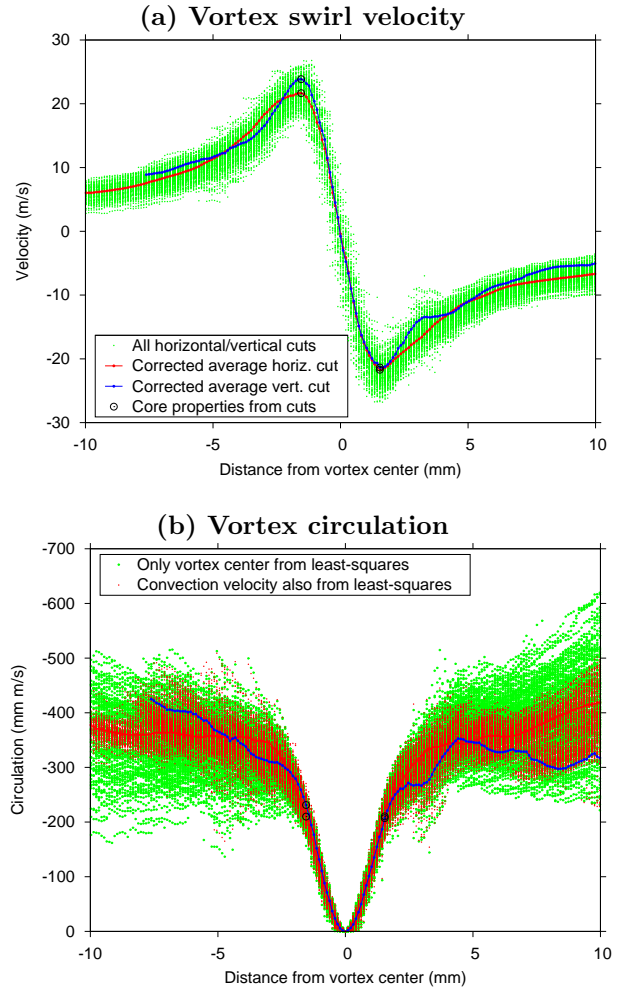
surement are used to determine vortex core properties.

Figure 13(b) shows the same measurements in terms of circulation profile. In this case the red symbols show the cuts through individual measurements, but with the convection velocity also obtained from the least-squares fit. This small additional information noticeably reduces the scatter in the data and highlights the benefits of using more measured data through the least-squares fit. The advantage of using all the measured PIV data was first identified in Ref. 15 where a fit to the Vatistas (Ref. 19) model was used to obtain the core properties. The obvious next step would be to not only identify the vortex center and convection velocity, but also the vortex core properties from the least-squares fit using the plane fit.

### Individual Average

The advantage of the least-squares fit is that it readily provides estimates of the core properties along with the vortex center location. This makes the individual average a simple next step where the core properties obtained from the individual measurements are averaged to give mean vortex core properties. This is shown in Fig. 14 in the form of normalized standard deviation of the estimated individual core properties. Similar variations reported in previous work are also shown for comparison along with the normalized vortex aperiodicity magnitude. The differences in the variation in calculated vortex properties between these different works can be attributed to two key differences: differences in obtaining the vortex center and differences in obtaining the vortex core properties.

Using a curve fit to determine the vortex center provided the least scatter in the estimated vortex properties, as seen from both the present work as well as the HART II results in Ref. 15. After the vortex center was



**Fig. 13. Measured swirl velocity and circulation distributions along horizontal and vertical cuts through the vortex center for both the instantaneous and the corrected average flow fields,  $C_T = 0.0$ ,  $\psi = 4$  deg.**

determined, Ref. 13 used only the peak swirl velocity along a one-sided cut through the vortex center to determine the core size. Ref. 9 used half peak-to-peak swirl velocity along a symmetric cut through the vortex center. Ref. 15 used a curve-fit similar to the present work. Comparison of the results from these three works suggests that the curve-fit is a better approach for determining the vortex core properties. To examine this further, the vortex core properties from the present measurements were estimated using these three methods. The results are shown in Fig. 15. All three results used the least-squares curve fit to determine the vortex centers. The results strongly suggest that using a curve-fit based approach is superior than using only the locations of the peak swirl velocities to determine the vortex core properties.

Even while using just the peak swirl velocity locations to determine core properties, using a curve-fit based approach to determine the vortex center gives improved results. This is clearly evident from the reduced scatter in vortex core properties for the present measurements de-

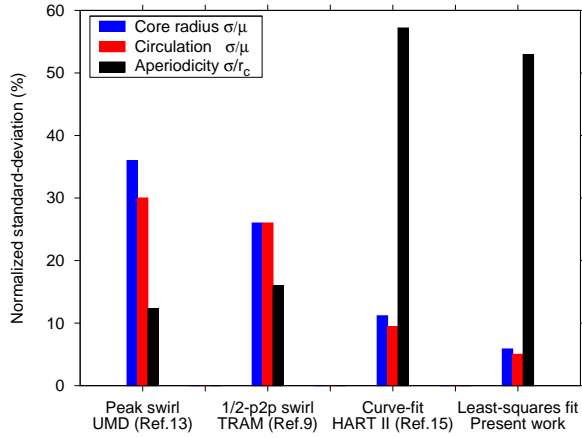


Fig. 14. Normalized variation in the vortex core properties obtained from individual average along with the vortex aperiodicity magnitude compared with previous works.

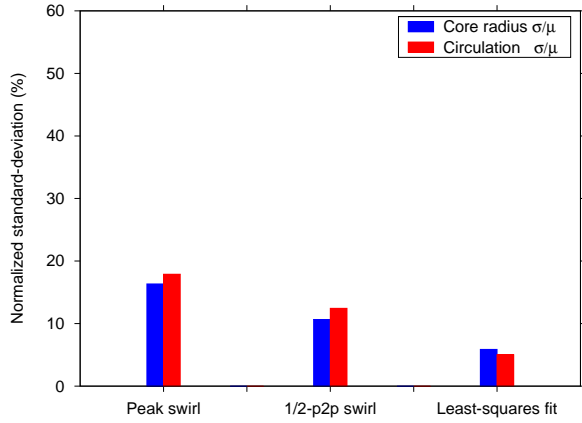


Fig. 15. Normalized variation in the vortex core properties obtained using different methods for the present measurements using individual average,  $C_T = 0.0076$ ,  $\psi = 4$  deg.

terminated from peak swirl velocity and half peak-to-peak swirl velocities as compared to Refs. 13 and 9, respectively.

To further illustrate the advantage of the least-squares fit over simply using the peak swirl velocity from cuts through the vortex center, two sample individual measured velocity profiles are shown in Fig. 16. Measurements along a cut through the vortex center are shown along with the velocity profile given by the least-squares fit to the entire measurement plane. In the first case, shown in Fig. 16(a), there is an asymmetric void near the vortex core. As a result, the core properties obtained from the peak swirl velocity along the line cut through the vortex is highly inaccurate. Note that in this case, even though the center was accurately determined based on the least-squares fit the core properties based on a line cut are still inaccurate, unless the estimated values from the curve fit are used. In Fig. 16b, there is one outlier present near the vortex center and this gives a

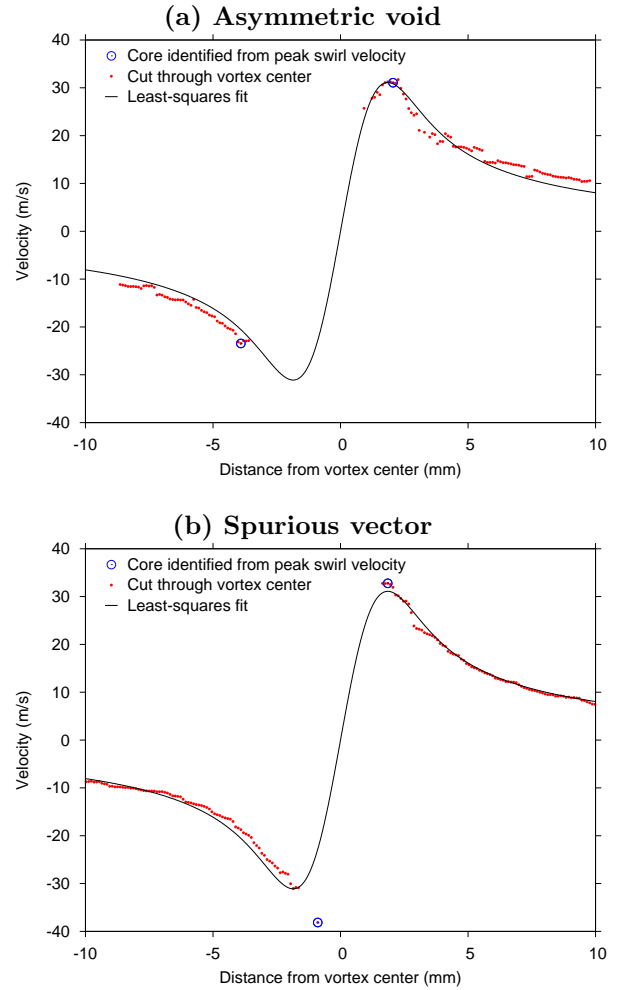
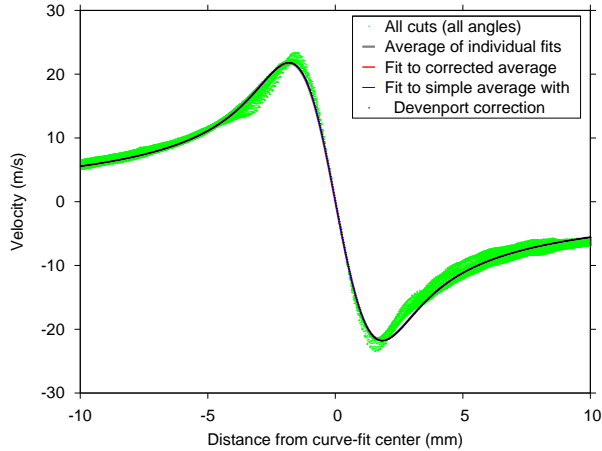


Fig. 16. Examples showing the advantages of the least-squares fit in the presence of: (a) Asymmetric void, and (b) Spurious measurements.  $C_T = 0.0076$ ,  $\psi = 4$  deg.

incorrectly large peak swirl velocity and a smaller core radius. The least-squares approach is not unduly biased because of this one outlier and can correctly estimate the vortex core properties. These two extreme examples demonstrate the reasons why previous work found very large variation in the core properties obtained from individual measurements (Ref. 9, 12).

The comparison of the results obtained using all three aperiodicity correction methods is shown in Fig. 17 in the form of swirl velocity distribution. Measurements obtained by making several cuts across the vortex from the corrected or conditional average (CA) flow field are also shown. Only data points with at least 50% samples are presented in the CA results. The plot also includes horizontal and vertical cuts from CA flow field, separately. The simple average (SA) results are corrected in a manner similar to Devenport et al. (Ref. 5) to give a smaller core radius but the same total vortex circulation. The individual average (IA) results are based on average of core radius and circulation obtained from all individual measurements using the least-squares approach. Two key



**Fig. 17. Comparison of the three methods for aperiodicity correction: simple average, corrected average, and individual average.**  $C_T = 0.0076$ ,  $\psi = 4$  deg.

observations can be made here. First, all three aperiodicity correction methods give the same results. Second, as expected, using a horizontal or vertical cut (or their average) may not provide accurate results even when using corrected average flow field. In this case, the peak swirl velocity obtained through the vertical cut lies on the far end of the scatter spectrum and can be seen to be farthest from the mean value.

### Example Results

Figure 18 shows all six vortex properties obtained from the least-squares fit for the  $C_T = 0$  case at a young wake age of approximately 4 degree (just behind the trailing edge). The vortex properties for all individual measurements are shown along with the mean properties obtained using the three aperiodicity correction methods. The CA and SA results are obtained by averaging all measurements, with and without aligning the vortex centers, respectively, and then obtaining the core properties. The vortex core size obtained using SA is also corrected using the analytical correction given by Devenport et al. (Ref. 5). Note that the vortex aperiodicity results in a larger apparent core radius and a small apparent peak swirl velocity, but the total vortex circulation (away from the core) remains unaffected. The scatter plot show the properties obtained using the least-squares fit for each individual measurement. The IA result is simply the mean of these individual results and is shown with one standard deviation.

In the present study the PIV measurement grid spacing was about 0.1 mm; Fig. 18a shows the standard-deviation in the vortex core radius is about half of one grid spacing. The circulation is negative because the tip vortex is rotating in a clockwise direction (opposite to the conventional counter-clockwise direction) for a negatively loaded tip. The vortex center locations show a larger scatter in the vertical ( $y$ ) direction compared to

the radial ( $x$ ) direction. The vortex convection velocities are radially inward and axially upward, and these result in a small deviation in the vortex axis away from the normal to the measurement plane. The least-squares fit already corrects for this orientation.

Figures 19 and 20 show the core radius and the vortex circulation for  $C_T = 0.0076$  at two wake ages: one at 4 degrees and one at 15 degrees. The core radius increases by about 50% between these early vortex ages whereas the total circulation only increased slightly suggesting that the vortex roll-up is nearly complete.

In all cases, the SA method gives a larger vortex core radius while the CA and IA methods closely agree with each other. Inclusion of a simple correction based on Devenport et al. (Ref. 5) approach in the SA result for the core radius makes it agree with the CA and IA results. All three results for other vortex parameters agree very closely with each other, i.e., they are all within one standard deviation of the mean IA result. This strongly suggest that all three methods for aperiodicity correction are equally valid and give consistently accurate results when applied carefully.

### Concluding Remarks

Three methods for aperiodicity correction were applied to microscopic PIV measurements in the wake of a hovering model scale rotor. The present approach was based on a least-squares fit of the measurements to a model vortex flow field. The approach was employed in three aperiodicity correction methods: the simple average, the corrected average or conditional average, and the individual average. All three methods were shown to give good estimates for the vortex core properties, and were consistent with each other. Specific conclusions are summarized below.

1. Accurate determination of the vortex center location is essential to the corrected or conditional average method for aperiodicity correction. The least-squares fit was shown to give accurate vortex center location even in the presence of an asymmetric seed void. Most importantly, the vortex center location was shown to be independent of the underlying vortex model used in the fit.
2. The background velocity was assumed to be constant within a measurement window and equal to the vortex convection velocity. The size of the measurement window was varied to ensure that the vortex core properties did not change with window size. The vortex convection velocity is influenced by the inclination of the measurement plane with respect to the vortex axis; this was included in the formulation before determining the vortex core properties.

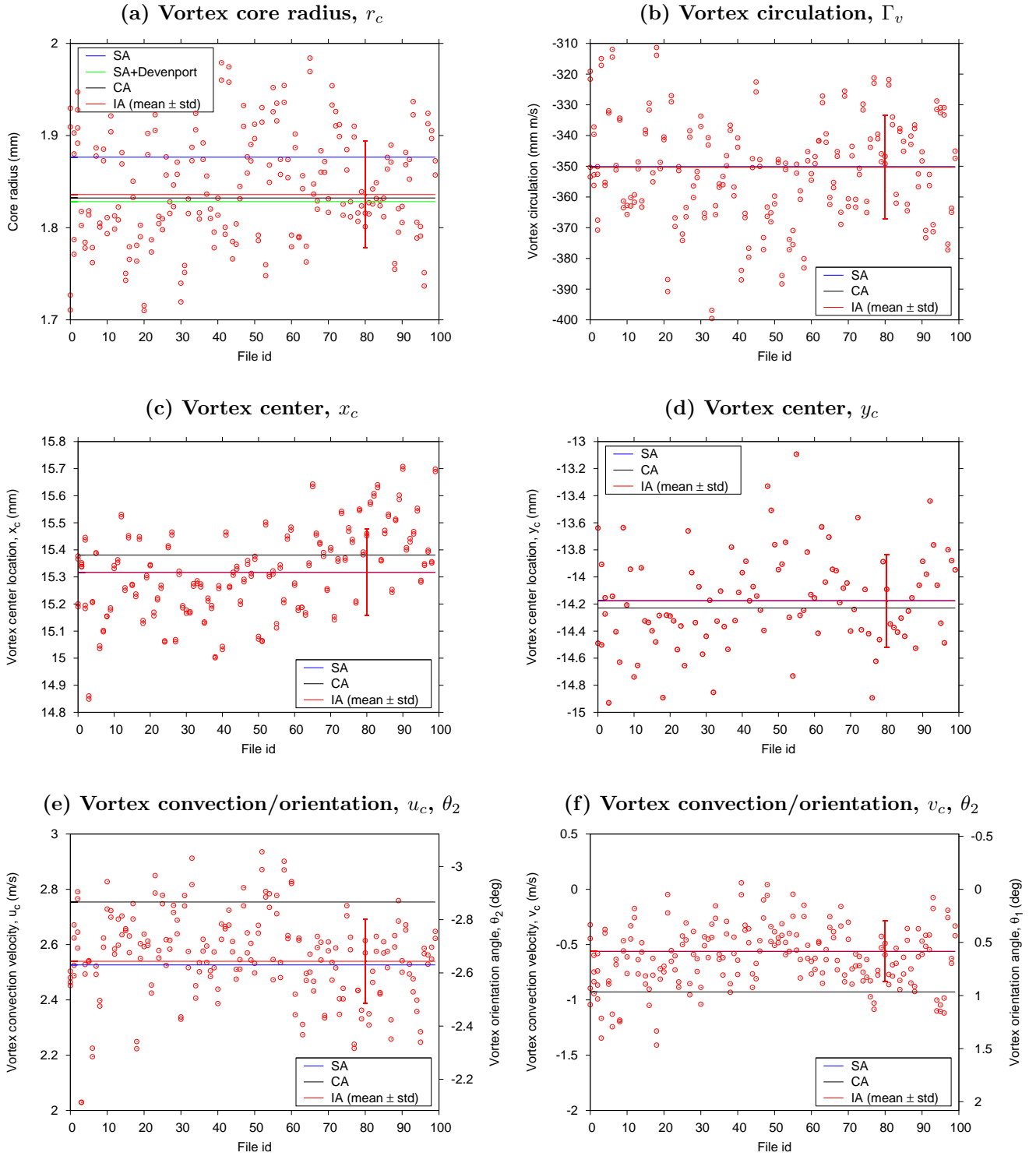
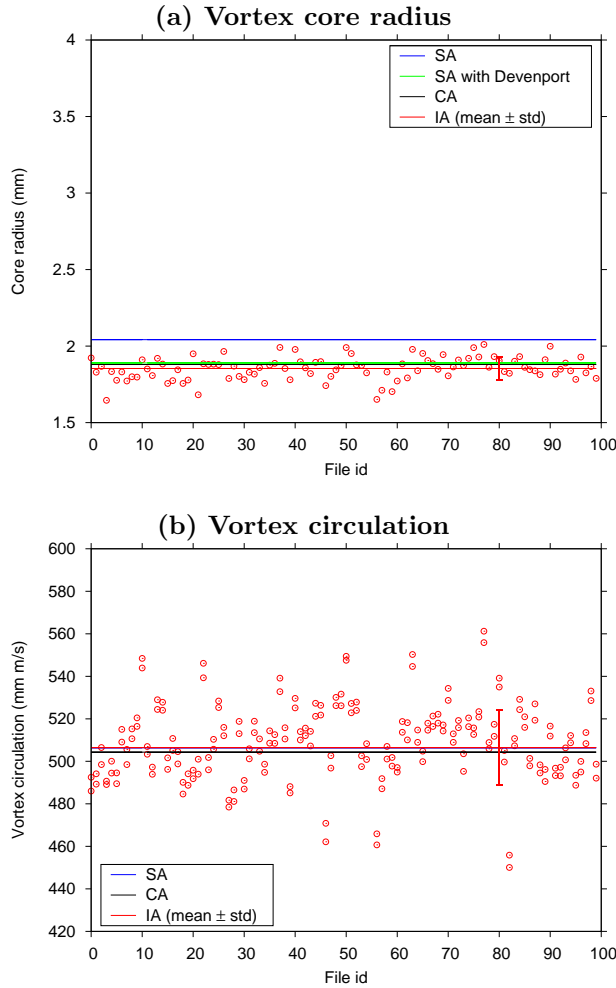


Fig. 18. Vortex core properties obtained using the least-squares fit,  $C_T = 0.0$ ,  $\psi = 4$  deg.

3. The vortex core properties were also obtained from the least-squares fit rather than using a few linear cuts through the vortex center. This ensured that most of the measured data contributed towards the vortex core properties instead of only a few points along the line cuts that resulted in more accurate estimation of these properties. Unlike line cuts, the present approach was not adversely affected by the lack of valid velocity vectors at the core boundary or by the presence of spurious vectors within the vortex core.
4. Even the simple average gave a good estimation of vortex core properties provided the core radius and peak swirl velocities were corrected using the inverse convolution of Davenport et al.. The mean vortex core properties estimated from all three aperiodicity correction methods (SA with Davenport correc-



**Fig. 19. Vortex core radius and vortex circulation for 100 individual measurements,  $C_T = 0.0076$ ,  $\psi = 4$  deg.**

tion, CA and IA) were self-consistent and well within one standard deviation of the individual measurements. Especially, the measured core size from all three methods was within the measurement resolution.

### Acknowledgements

The authors gratefully acknowledge the discussions with Drs. Gloria Yamauchi and Alan Wadcock that were particularly helpful in clarifying the vortex orientation and convection in the least-squares fit.

### References

- [1] Takahashi, R. K. and McAlister, K. W., "Preliminary Study of a Wing-Tip Vortex Using Laser Velocimetry," Technical Report TM 88343, NASA, January 1987.
- [2] Martin, P. B., Pugliese, G., and Leishman, J. G., "High Resolution Trailing Vortex Measurements in the Wake of a Hovering Rotor," Proceedings of the

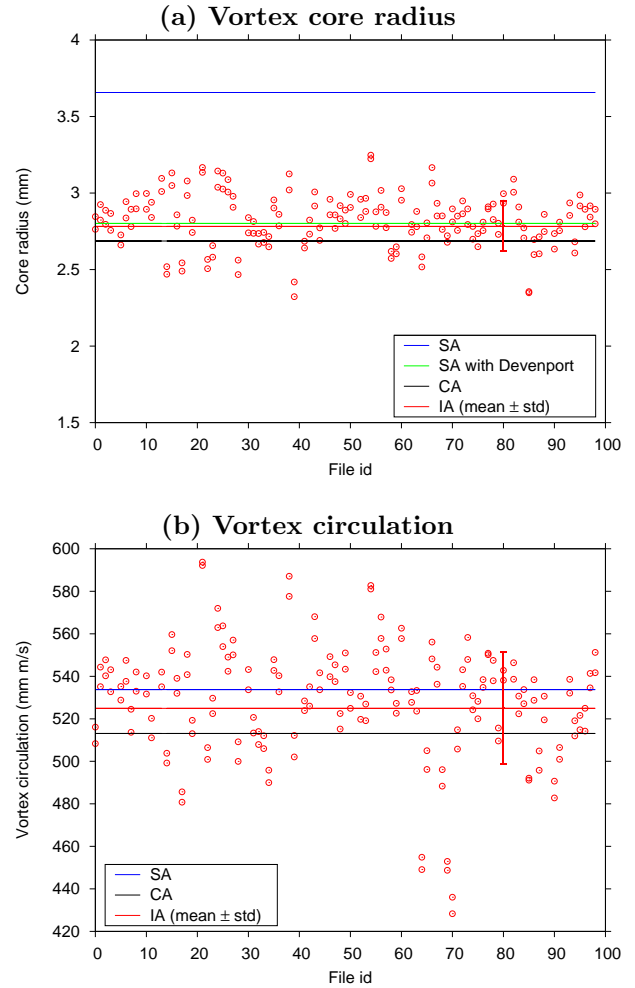


**Fig. 20. Vortex core radius and vortex circulation for 100 individual measurements,  $C_T = 0.0076$ ,  $\psi = 15$  deg.**

American Helicopter Society 57th Annual National Forum, Washington, D. C., May 9–11, 2001.

- [3] Ramasamy, M. and Leishman, J. G., "Interdependence of Diffusion and Straining of Helicopter Blade Tip Vortices," *Journal of Aircraft*, Vol. 41, (5), September 2004, pp. 1014–1024.
- [4] Devenport, W. J., Rife, M. C., Liapis, S. I., and Miranda, J. A., "Turbulent Trailing Vortices," Paper AIAA-94-0404, Proceedings of 31nd Aerospace Sciences Meeting & Exhibit, Reno, NV, January 10–13 1994.
- [5] Devenport, W. J., Rife, M. C., Liapis, S. I., and Follin, G. J., "The Structure and Development of a Wing-Tip Vortex," *Journal of Fluid Mechanics*, Vol. 312, 1996, pp. 67–106.
- [6] Lamb, H., *Hydrodynamics*, Cambridge University Press, Cambridge, UK, 6th edition, 1932, pp. 592–593.
- [7] Oseen, C. W., "Über Wirbelbewegung in Einer Reibenden Flüssigkeit," *Ark. J. Mat. Astrom. Fys.*, Vol. 7, (Nonumber), 1912, pp. 14–21.

- [8] Leishman, J. G., “Measurements of the Aperiodic Wake of a Hovering Rotor,” *Experiments in Fluids*, Vol. 25, (4), September 1998, pp. 352–361.
- [9] Yamauchi, G. K., Burley, C. L., Mercker, E., Pengel, K., and JanakiRam, R., “Flow Measurements of an Isolated Model Tilt Rotor,” Proceedings of the American Helicopter Society 55th Annual National Forum, Montreal, Canada, May 25–27 1999.
- [10] Vogt, A., Baumann, P., Kompenhans, J., and Gharib, M., “Investigations of a Wing Tip Vortex in Air by Means of DPIV,” Paper AIAA-96-2254, Proceedings of the 19th AIAA Advanced Measurement and Ground Testing Technology Conference, New Orleans, LA, June 17–20 1996.
- [11] Heineck, J. T., Yamauchi, G. K., Wadcock, A. J., Lourenco, L., and Abrego, A. I., “Application of Three-Component PIV to a Hovering Rotor Wake,” Proceedings of the American Helicopter Society 56th Annual National Forum, Virginia Beach, VA, May 2–4 2000.
- [12] Ramasamy, M., Johnson, B., Huismann, T., and Leishman, J. G., “A New Method for Estimating Turbulent Vortex Flow Properties from Stereoscopic DPIV Measurements,” Proceedings of the American Helicopter Society 63rd Annual National Forum, Virginia Beach, VA, May 1–3 2007.
- [13] Ramasamy, M., Leishman, J. G., and Lee, T. E., “Flow Field of a Rotating Wing MAV,” *Journal of Aircraft*, Vol. 44, (4), July 2007, pp. 1236–1244.
- [14] Ramasamy, M., Johnson, B., and Leishman, J. G., “Turbulent Tip Vortex Measurements Using Dual-Plane Stereoscopic Particle Image Velocimetry,” *AIAA Journal*, Vol. 47, (8), July 2009, pp. 1826–1840.
- [15] van der Wall, B. G. and Richard, H., “Analysis Methodology for 3C-PIV Data of Rotary Wing Vortices,” *Experiments in Fluids*, Vol. 40, 2006, pp. 798–812.
- [16] Ramasamy, M., Gold, N., and Bhagwat, M. J., “Flowfield Measurements to Understand Effect of Wake Behavior on Rotor Performance,” AIAA-2010-4237, Proceedings of the 28th AIAA Applied Aerodynamics Conference, Chicago, IL, Jun 28–30 2010.
- [17] McAlister, K. W., “Rotor Wake Development During the First Revolution,” Proceedings of the American Helicopter Society 59th Annual National Forum, Phoenix, AZ, May 6–8 2003.
- [18] Leishman, J. G., “Seed Particle Dynamics in Tip Vortex Flows,” *Journal of Aircraft*, Vol. 33, (4), July 1996, pp. 823–825.
- [19] Vatistas, G. H., Kozel, V., and Mih, W. C., “A Simpler Model for Concentrated Vortices,” *Experiments in Fluids*, Vol. 11, (1), April 1991, pp. 73–76.
- [20] Iversen, J. D., “Correlation of Turbulent Trailing Vortex Decay Data,” *Journal of Aircraft*, Vol. 13, (5), May 1976, pp. 338–342.
- [21] Ramasamy, M. and Leishman, J. G., “A Generalized Model for Transitional Blade Tip Vortices,” *Journal of the American Helicopter Society*, Vol. 51, (1), January 2006, pp. 92–103.
- [22] Ramasamy, M. and Leishman, J. G., “A Reynolds Number Based Rotor Blade Tip Vortex Model,” *Journal of the American Helicopter Society*, Vol. 52, (3), July 2007, pp. 214–223.